

Nanocluster topological engineering of thin films by laser-hybrid technologies

S.M. Arakelian*, A.O. Kucherik, T.A. Khudaberganov, D.N. Bukharov,
O.Ya. Butkovsky

*Department of Physics and Applied Mathematics, Vladimir State University,
Gorky Str. 87, 600000 Vladimir, Russia, arak@vlsu.ru

Corresponding Author: Tel.: +7-4922-33-33-69 ; E-mail address: arak@vlsu.ru

-----ABSTRACT-----

This paper discusses a number of issues of laser and laser-hybrid technologies that can be used with intelligent modern laser technological complexes to obtain composite materials of different elements composition. We are talking about the following new physical principles based on laser methods of surface treatment of various materials controlled in the required direction with micro- nanostructures and hydrodynamic instabilities.

The paper also presents experiments on crystallization of complex structures from a melt with an analysis of the morphology of the resulting crystalline structures, and shows examples of the occurrence of fractal dendritic formations. Different types of morphology are induced depending on the energy of the laser radiation and the duration of the heating determining the final state of objects with the desired functional and structural characteristics.

These new physical principles of today's laser technologies with new generation of intelligent laser technological complexes are discussed on the basis of the actual experimental results obtained, and its analysis we present in the framework of certain dynamic models.

KEYWORDS; 4D-laser technologies, controllable surface topological structures, nanostructures engineering of the thin film systems

Date of Submission: 06-07-2020

Date of Acceptance: 21-07-2020

I. INTRODUCTION

The uniqueness of laser technology is primarily determined by the synthesis of micro-nanostructured surface layers of different elements composition with a certain topology and with variable dimensional parameters for different durations of laser pulses (from continuous to femtosecond), which play a fundamental role for the needs of various applied problems, especially in aspect of the use of critical parts of mechanical engineering. Such 4D-technologies (firstly, with a spatial component, depending on the emerging laser-induced surface spatial structure, and secondly, with a temporary component – a variable time of laser irradiation to implement specific mechanisms of laser exposure to materials) have no competitive analogues for today. Here, at first glance, a paradoxical result arises when monolithic products have performance characteristics worse than the same products with laser-induced inhomogeneous/granular structures on their surface, synthesized by controlled methods and in a necessary direction (cf. [1]).

II. TOPOLOGICAL STRUCTURES ON THE SURFACE OF MATERIALS

Let us present the obtained images for laser-induced structures under various modes of action on the surface of objects.

In Fig. 1 it is shown the optical images of a characteristic cavity formed on the surface of glassy carbon when exposed to laser radiation of power P ; exposure time is $t=2s$. In these images, two areas can be distinguished whose properties differ significantly. The number 1 indicates the zone of direct laser exposure: the surface of this area is smooth, without a noticeable relief. The number 2 indicates the zone of ring formations at the boundary of the laser exposure region and beyond. Visually in an optical microscope, this area has a characteristic matte gloss. As further, more detailed studies using atomic force microscopy have shown, nanostructures of various shapes and sizes with a certain distribution over the surface are observed in these zones [2,3]. In zone 1, structures of the «stalagmite» type were observed – dips in the surface (see Fig. 2). Zone 2 is characterized by the formation of structures in the form of «nanopeaks» (see Fig. 3).

It can be noted that the size of structures of the «stalagmites» type is heterogeneous and ranges from 0.08 to 5 μm at the base. Moreover, their average longitudinal size reaches 200-400 nm. Discovered within the zone 2 of the formation of «nanopeaks» have a base diameter of 0.4-0.5 μm , a height of 60-300 nm and are

disparate structures at the central ring. Towards the outer edge there are more compacted formations with a lower height, but larger in size base. The presented type of caverns after laser exposure is characteristic for this type of material.

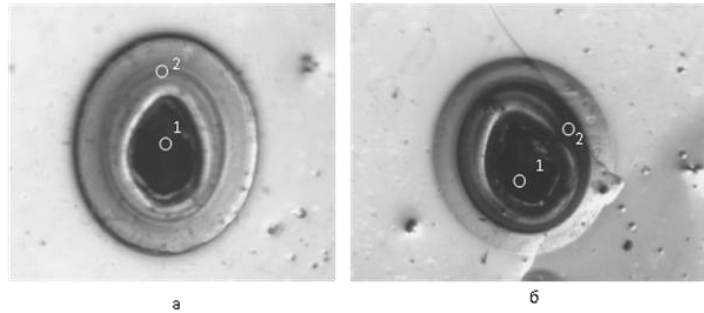


Fig. 1: Image of caverns on the surface of glassy carbon with an optical magnification of (x28): a) $P = 30\text{ W}$, $t=2\text{s}$; b) $P = 76\text{ W}$, $t=2\text{s}$. Explanations are given in the text.

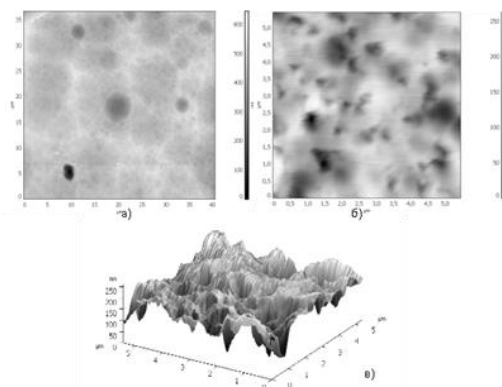


Fig. 2: AFM-image of the laser exposure region in zone 1 of Fig. 1. Characteristic «gaps» in the structure of the surface of glassy carbon are observed:
 a) relief of the 2D-surface, $t = 2\text{ s}$, $P = 30\text{ W}$;
 b) relief of the 2D-surface, $t = 2\text{ s}$, $P = 76\text{ W}$;
 c) 3D-relief of the surface shown in Fig. b).

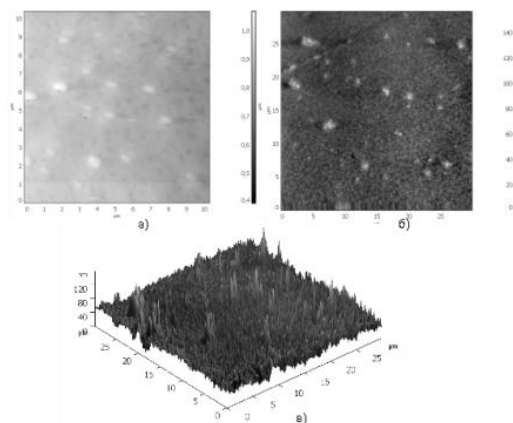


Fig. 3: AFM- image of the laser exposure region in zone 2 of Fig. 1. The characteristic formation of «peaks» in the structure of the surface of glassy carbon is observed:
 a) relief of a 2D-surface, $t = 2\text{ s}$, $P = 30\text{ W}$;
 b) relief of the 2D-surface, $t = 2\text{ s}$, $P = 76\text{ W}$;
 c) 3D-relief of the surface shown in Fig. b).

With an increase in the laser irradiation time $t > 3\text{ s}$, an increase in the number of typical zones was observed (see Fig. 4, zones 1–3). Moreover, in contrast to Fig. 1 there is a change in their parameters: radial

size, the depth of the central zone of the cavity, the elevation of the relief of zones 2,3 as well as the formation of faults in zone 1.

In zone 1 of Fig. 4, as in the case considered earlier, with shorter exposure times, structures of the «stalagmites» type arise. A significant difference is the stabilization of the transverse size of structures similar to each other (see Fig. 5). Due to the high repeatability of the structures, their image resembles the formation of nanograins on the surface of materials processed at high power. In this case, the formation of such characteristic «domains» on an amorphous surface can be associated with the melt crystallization process. An increase in the transverse dimensions of the «domains» from 1.5 μm to 2 μm was observed, depending on the duration of the laser irradiation.

In zone 2 of Fig. 4, the formation of «nanopeaks» was discovered that repeat the types of nanostructures of samples with shorter exposure times; at the same time, their base is 0.3-0.5 μm , and the height is 300-600 nm (see Fig. 6). At the boundary of the laser irradiation region, nanostructures more sparse in spatial distribution were also observed.

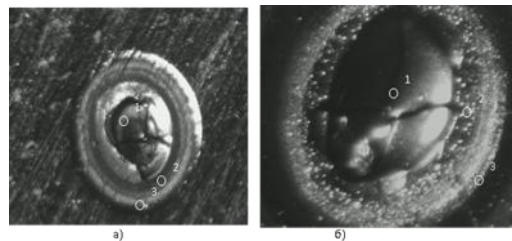


Fig. 4: Image on the surface of glassy carbon cavities with optical magnification (x28): a) $P = 76 \text{ W}$, $t = 6 \text{ s}$; b) $P = 76 \text{ W}$, $t = 10 \text{ s}$. Characteristic zones 1-3 are shown.

Zone 3 in Fig. 4 is the boundary of the undisturbed and irradiated zones of the sample. At exposure times of the order of 3-4s this region does not contain pronounced features (Fig. 6(d)).

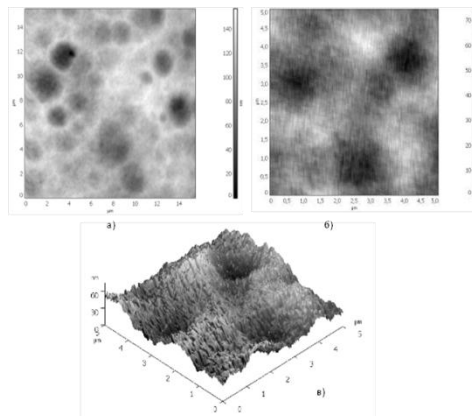


Fig. 5: AFM-image of the laser exposure region of zone 1 of Fig. 4. The characteristic domains on the surface of glassy carbon are observed:

- a) relief of the 2D-surface, $t = 3 \text{ s}$, $P = 76 \text{ W}$;
- b) relief of the 2D-surface, $t = 6 \text{ s}$, $P = 76 \text{ W}$;
- c) 3D-relief of the surface shown in Fig. b).

With an increase in the exposure time (more than 5 s), a «transition region» can be distinguished on the surface of the samples. This area has well-defined boundaries; its diameter depends on the power and time of exposure to laser radiation (see. Fig. 7). Its distinctive feature is the ability to detect the initial relief of the sample under «neoplasms» (see Fig.8 (a, b, c)). The nature of the occurrence of such an area is ambiguous. Possibly, the process of its formation is associated with the deposition of hot material vapors leaving the region of laser exposure. It can be argued that the solid-phase destruction of the surface under the influence of thermal stresses due to laser irradiation in this case is not the dominant mechanism, since the original relief is preserved.

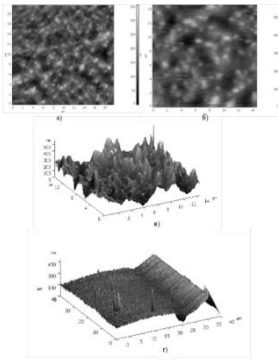


Fig. 6: AFM-image of the laser exposure region in zone 2 of Fig. 4. Typical glassy carbon domains: a – 2D-surface topography, $t = 3\text{ s}$, $P = 76\text{ W}$; b – 2D-surface relief, $t = 6\text{ s}$, $P = 76\text{ W}$; c – 3D-relief of the surface shown in Fig. b, $t = 3\text{ s}$, $P = 76\text{ W}$. The same figure (d) shows a 3D-relief of the surface outside the laser irradiation region (region 3 in Fig. 4): $t = 3\text{--}4\text{ s}$, $P = 76\text{ W}$.

Indeed, AFM-studies did not allow us to determine the preferred direction of propagation of this effect. Therefore, it is necessary to follow the processes of surface melting of the material when the liquid phase of carbon flows out towards the formed penetration channel (cf. [4]).

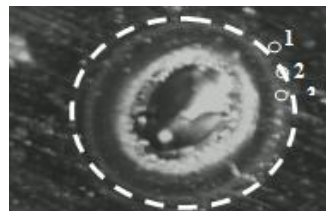


Fig. 7: Image of a cavity on a glassy carbon surface under laser exposure with an optical magnification of (x28): $P = 76\text{ W}$, $t = 5\text{ s}$. The transition region is indicated by a dashed line. At points 1, 2, and 3, AFM-images were obtained, which are shown below in Fig. 8.

Thus, for different conditions of laser exposure (exposure time and its power), it is possible to excite various structures on the surface of glassy carbon. These characteristic features of the recorded images are usually universal for other solid materials in similar modes under laser action with melting.

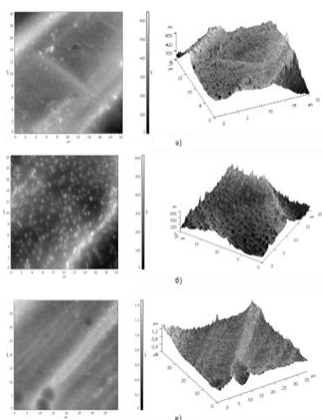


Fig.8: AFM-images of characteristic zones of Fig. 7 for glassy carbon: 2D-images on the left and 3D-images on the right. The following are observed: a) at point 1 – characteristic formations of the «nanopeaks» group (the initial relief is noticeably traced); b) at point 2 – the characteristic formations of the group of «nanopeaks» (the initial relief is not traced); c) at point 3 – the characteristic formations of the «nanopeaks» group (the initial relief is again traced).

Finally, let us consider shortly the conditions under which complex fractal formations (classical dendrites) can form on the surface of a steel under the influence of laser radiation. In this case, the distribution of dendrites over the surface of the laser irradiation zone can be controlled by changing the profile/shape of the laser beam cross section (with a convex weld structure). Using electron microscopy, we also estimated both the size distribution of dendrites and the density of their distribution over the surface.

Experimental results (Fig. 9) show that with longer heating in the peripheral areas of exposure, a greater number of stable crystallization centers arise: the more centers, the greater the energy and duration of the laser exposure with a constant radiation power density. In this case, the fractal structure indicates the uneven nature of the temperature distribution during the occurring phase transition. The crystals formed differ in shape: on the very edge of the area of influence, «needle-like» formations (spherulites) are noticeable; closer to the center, the crystals take on a form similar to the classical stochastic fractal. The size of the formed dendrites, as already noted, ranges from 0.07 to 3.0 μm with an average size of 1.19 μm, but in different zones of the area of influence the average size of dendrites is the same. «Isolated» dendrites reached sizes up to 3 μm. With a longer laser exposure, in addition to increasing the number of crystals, their size also increased, reaching 9 μm. Spherulites were even larger – up to 19 μm. To analyze the geometric dimensions of the crystal, atomic force microscopy was used. Crystals are formed in the surface layer of the material (the height in the center is about 1 μm, decreases along the directions to the periphery). We can conclude that at the beginning a stable nucleus of a new crystalline phase is formed, and then its branches «grow» under the influence of diffusion. These assumptions determine the approaches to the interpretation of experimental data, and the development of two-dimensional theoretical models, e.g. by cellular automation for discrete dynamic system.

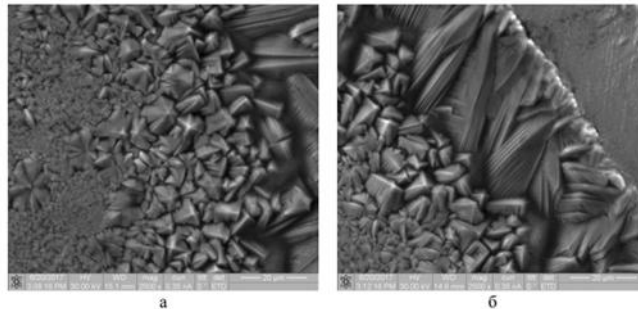


Fig. 9: A group of dendrites and spherulites in the periphery of the region of laser irradiation on the surface of the material with laser pulse parameters (power/duration) of 14 J / 14 ms (left) and 16 J / 16 ms (right). The scale of the SEM-images is 20 μm.

III. SPECTRAL CHARACTERISTICS OF NANOCLUSTER SYSTEM

Different topological structures for nanoobjects, obtained by computer simulation in arbitrary units in spherical coordinate system (R, φ, θ), were modeled by us.

From the very beginning the shape of the body was spherical (radius R₀) which is perturbed by variation of some key parameters: the ratio of the values of both azimuthal (k₁) and zenithal (k₂) distortions (0 ≤ k₁ ≤ 1, 0 ≤ k₂ ≤ 1, respectively); as well as the number of distortions for the same parameters (p₁ = 0, 1, 2, ... ; p₂ = 0, 1, 2, ...). The approach is shown by formula (1):

$$R(\theta, \phi) = \begin{cases} R_0 \left[\begin{aligned} & \left[(1 + k_1 \cos(\theta) \cos(p_1 \phi)) + \right. \\ & \left. + k_2 \left((-1)^{\frac{p_2-1}{2}} \text{mod}(p_2, 2) \sin(p_2 \theta) + \text{mod}(p_2 + 1, 2) \cos(p_2 \theta) \right) \right] \right], p_1 \neq 0, \\ R_0 k_2 \left((-1)^{\frac{p_2-1}{2}} \text{mod}(p_2, 2) \sin(p_2 \theta) + \text{mod}(p_2 + 1, 2) \cos(p_2 \theta) \right), & p_1 = 0. \end{aligned} \right. \quad (1)$$

We analyzed the following cases for the deformation parameters: k₁=k₂=0.4 and p₂ = 0, 1, 2, ...; p₁ = 0, 1, 2. Soft Mathcad programming has been used for the modeling.

Several selected results in accordance with formula (1) are shown in Fig. 10(a).

The energetic parameters, relying on the fact that the obtained nanoobject complex structures result in the modification of the potential energy distribution for quantum wells, and therefore can be discussed in a standard quantum mechanics approach.

In the case the energy levels are split as follows (see Fig. 10(b)). We used the simplest case in approximation of the first order linearization in the small deformations vs geometric parameters which result in perturbation of the energy levels as

$$\delta E_{n,l,m} = \int_0^{2\pi} \int_0^\pi \int_0^{R_0} \Psi_{n,l,m}^* (r, \theta, \phi) \delta H \Psi_{n,l,m} (r, \theta, \phi) r^2 \sin \theta dr d\theta d\phi (2)$$

where n, l, m are the standard quantum numbers in the atomic spectrum of quantum system, δH – perturbation of Hamiltonian, ψ – wave function.

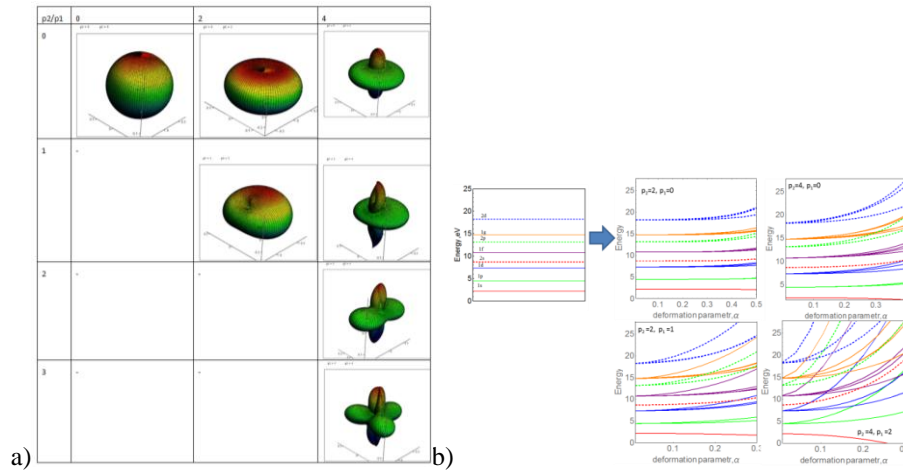


Fig.10:(a) Several topological structures controlled by the key parameters (see text). (b) Spectra of deformed nanoclusters. The split energy levels are shown for different distortions when we fixed $k_1 = k_2 = a$ and variable magnitudes of p_1, p_2 . Numerical parameters are: valent electron density $N_e=40$; Wigner-Seitz parameter $r_s=2.1$ ($\sim 1/N_e^{1/2}$); electron effective mass $m_{eff}^* = 1.4m_e = 0.708MeV$.

Thus, by changing the topology of nanoparticles we can modify the energetic levels of the optical system. The fact plays a principal role for the nanophotonics device application. Table 4(for depth 4)

IV. ELECTROCONDYCTIVITY OF A GRANULATED METALLIC FILMS

Quantum mobility of electrons over different trajectories in a spatially inhomogeneous structure (see Fig.11b), i.e. in a nanocluster network system, may be presented in accordance with the path integral-theory approach [5].

We analyzed the problem in frame of standard model of harmonic oscillator (with frequency ω and quantum numbers l, m) in external electric field E with offset $(x - x_{lm})$ in the one-dimensional case. In the case, the propagator K is:

$$K = \langle q'' | U(t'', t') | q' \rangle = \int \exp\left(\frac{i}{\hbar} \int_{t'}^{t''} L dt\right) Dq, \quad (3)$$

with U as an evolution operator, $Dq = \frac{1}{A} \prod_{j=1}^{n-1} \frac{1}{A} dq_j(t_j)$ is a path integral measure, and Lagrangian L is represented in quadratic form:

$$L = \frac{1}{2} \sum_{l,m} \left\{ \frac{x'^2}{2N} - \omega^2 (x - x_{lm})^2 + Ex \right\}, \quad (4)$$

A – cross-section of the structure, n – number of the time sections due to fragmentation (over j) of $(t' - t'')$ -interval (using the transfer matrix approach [6]).

Further, we split the integral of action S of the path integral (3) into time slices with the step equal to Δt (divide the total time T of the particle motion by steps, $n\Delta t = T$):

$$S = \int_0^T L dt = \lim_{\Delta t \rightarrow 0} \Delta t \sum_{i=0}^n L(x_i) = \frac{1}{2} \lim_{\Delta t \rightarrow 0} \sum_{i=0}^n \sum_{l,m} \left\{ \frac{(x_{i+1} - x_i)^2}{2\Delta t N} - \omega^2 \Delta t (x_i - x_{lm})^2 + E \Delta t x_i \right\}. \quad (5)$$

Substituting (5) in the propagator (3) and moving to the Euclidean action through Wick-Rotation of time (this is a replace a time to imaginary time $\tau=it$), we get:

$$K(x_b, L, t_b; x_a, 0, t_a) = \int e^{-S_E[x_b, L, x_a, 0]/\hbar} DxDy = \int \prod_{j=0}^{n-1} e^{-H[j+1, j]\Delta t/\hbar} DxDy, \quad (6)$$

where $H[j+1, j] = H\left[\frac{x_{j+1}+x_j}{2}, \frac{x_{j+1}-x_j}{\Delta t}, \frac{y_{j+1}+y_j}{2}, \frac{y_{j+1}-y_j}{\Delta t}, -i(j+1/2)\Delta t\right]. \quad (7)$

Then, electrical conductivity has the form (cf.[7,8]):

$$\langle I \rangle = eS \int_0^{p_F} \frac{\hbar k}{m^*} \iint_0^{l_x} P(x_b, l_y, x_a, 0; E(k)) dx_a dx_b \frac{2\pi(p_F^2 - \hbar^2 k^2)}{(2\pi\hbar)^3} \hbar dk, \quad (8)$$

where $(x_b, l_y, x_a, 0; E(k)) = \int_0^\infty e^{-E\tau/\hbar} K(x_b, l_y, x_a, 0, \tau) d\tau$,

$\frac{2\pi(p_F^2 - \hbar^2 k_z^2)}{(2\pi\hbar)^3} \hbar dk$ – number of electrons at a Fermi sphere, and here now S – is the area/cross-section of the structure.

For specific nanostructures the numerical estimates of the electrical current should be made according to the relations (6)-(8). But the problem is not simple, and we briefly discuss it in conclusion.

Our results for electrical conductivity were obtained in the simple model of Kronig-Penney [7]. We analyzed the electroconductivity in frame of such quasi 1D-model of 10 nanoclusters for three key-processes: variation of energetic potential-scheme (Fig.11), electron-transmission (Fig. 12) and Volt-Ampere characteristics (Fig.13).

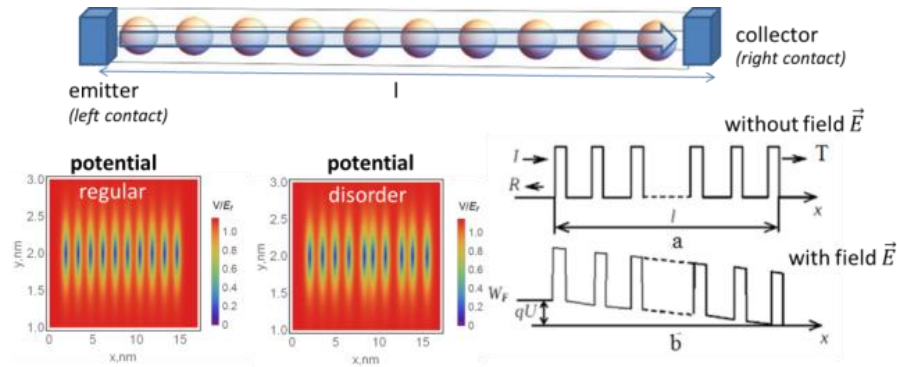


Fig. 11: Electric quantum tunneling through 10 nanoclusters (Kronig-Penney 1D-model). A potential form of the quasi-1D (Kronig-Penney like) nanocluster array (nanocluster superlattice) in both ordered and disordered cases (on the left). Schematic image of the nanocluster superlattice potential –on the right: top – without current (a); and bottom – with applied voltage U (b). For calculation, we used transfer matrix approach with Morse potential $V(r) = D_e(1 - e^{-a(r-r_0)})^2$, where D_e – depth of the potential well; $a = \omega_0\sqrt{m_e/2D_e}$ – width of the potential well; ω_0 – frequency of harmonic oscillator; r_0 – local minimum position (equilibrium state).

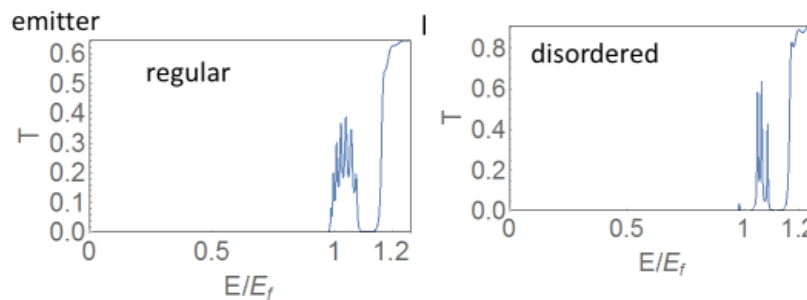


Fig. 12: Transmittance (T) of electrons in a quasi 1D-structure of nanoclusters as a function of the electron energy E for the regular (left) and disordered (right) structure (E is in the Fermi energy E_F units). The transmission spectrum of superlattice is split into a number of spectral bands. The numerical values: quantum-mechanical tunneling of electrons can occur both into the nanocluster and from the nanocluster into a neighbored nanoclusters. Resonant tunneling refers to tunneling in which the electron transmission coefficient through a structure is sharply peaked about certain energies (see nomination for the parameters in Fig.10): $N_e = 40, r_s = 2.1, m_e^* = 0.708MeV, E_F \approx 6eV, \frac{\hbar}{\tau} = 10^{-3} E_F, l$ – cluster/quantum well size $\approx 20nm$.

For the electrons with the energy corresponding approximately to the virtual resonant energy level of the quantum well, the transmission coefficient is close to unity. That is why an electron with this resonant energy can cross the potential barrier without being reflected. This resonant phenomenon is similar to that taking place in the optical Fabry-Perot resonator or in a microwave capacitively-coupled transmission-line resonators.

The final principal result is presented in Fig.13. It depends on the relationship between the electron energy (E) and Fermi-energy (E_F).

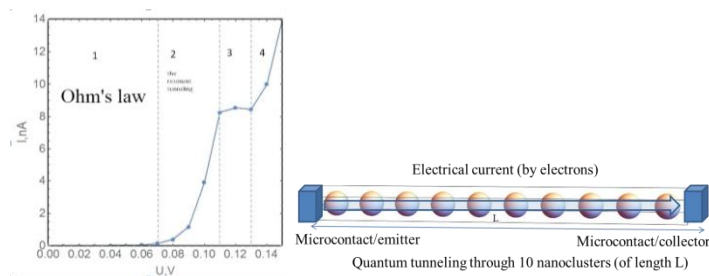


Fig. 13: Different regimes of electroconductivity in cluster systems (for Kronig-Penney model of superlattice – see below). Vertical axis – current I , horizontal axis – voltage U . The values of the numerical parameters are the same as in Fig.12; $E_F = 6\text{eV}$.

Region 1 with tunneling conductivity – shown on a small scale – is a dependence in accordance with approximately Ohm's law. With the positive charge shift to the right microcontact relative to the left one due to the applied voltage, the level of Fermi energy (E_F) on the left corresponds to the resonant level. This leads to a significant increase in current (region 2). With a larger value of the charge bias, the current stops flowing when the E_F level falls below the edge of the width of the conduction band. The result is a noticeable decrease in the current value with increasing voltage, which corresponds to the emergence of a region of negative differential resistance and/or a mode with significant current suppression (region 3). With a larger value of the charge displacement, the current increases again as the charged particles (electrons) acquire a sufficient kinetic energy (region 4).

For the case, electrical current J is defined as [8]:

$$J = eS \int_0^{p_F} \frac{\hbar k_z}{m^*} T(k_z) \frac{2\pi (p_F^2 - \hbar^2 k_z^2)}{(2\pi\hbar)^3} \hbar dk_z, \quad (9)$$

where S – a cross-section area of the structure, p_F – Fermi momentum, $T(k_z)$ – transfer matrix for transmission coefficient.

V. ELECTROCONDUCTIVITY OF A GRANULATED METALLIC FILMS

In the problem of controlling the functional properties of various materials during both the formation of nano-microstructures on the surface of solids and the deposition of thin films, the varying size parameters/topology scales of the formed nanostructures are important, which are determined by laser-induced dynamic instabilities (in both space and time). The emergence of such micro- and nanoperiodic/granular fixed objects, as well as the excitation of multistable stochastic dynamic states, including the formation of fractal spatial nonlinear images, the development and control of which in time under laser exposure, allows you to create final products with the required functional and structural characteristics.

In this case, sequential laser heating, the melt of the material and its further cooling can be realized when exposed to from continuous laser radiation to pulsed radiation, up to nanosecond durations, with the formation of structures with a spatial scale from several microns to several tens of nanometers. For laser pulses of shorter duration (from nanoseconds to femtoseconds), the mechanisms of synthesis of nanostructures are associated with the release of matter under laser irradiation – laser ablation; they lead to nanostructures with characteristic sizes from several tens of nanometers to 10 nanometers. Here we can talk about their formation both on the irradiated surface (target) itself, and during the deposition of matter on an additional target made of different materials located under controlled conditions and experimental geometries. In femtosecond technologies, it is possible in principle to control the electron-phonon states in crystalline samples with the achievement of variable and spatially distributed optical and electrophysical characteristics of the samples under the operating conditions of the products realized in industry and technology.

In particular, for the problem of high-temperature superconductivity, we are talking here about new mechanisms of the formation of bound electrons (Cooper pairs), but not due to the standard phonon mechanism (see, for example, [9]), and because of topological features by analogy with topological insulators (see. [10]). The development of these approaches is the subject of our further research. Fundamental in this case is the analysis of the possibility of achieving superconducting states – due to the optimal choice of the corresponding elements composition for such structures (cf. [11]), although we considered now, as the first stage, only simple combinations of elements from noble metals [12].

It is hoped that all these problems will certainly be solved in the very near future and will be in demand in the high-tech manufacturing sectors of the industry with the help of the corresponding new-generation laser

technological intelligent complexes using both laser-hybrid technologies and the fundamental achievements of modern femtonanophotonics.

ACKNOWLEDGEMENTS

This work was carried out within the framework of the Agreement between the Vladimir State University and the Russian Ministry of Education and Science № 075-15-2019-1838.

REFERENCE

- [1]. Arakelian S. M., Kucherik A. O., Prokoshev V. G., Rau V. G., Sergeev A. G. Introduction to femtonanophotonics. Fundamental and laser methods of controlled production and diagnostics of nanostructured materials.-M.: Logos; 2015. 744 p.
- [2]. Abramov D.V., Gerke M.N., Kucherik A.O., Kutrovskaya S.V., Prokoshev V.G., Arakelian S.M. The formation of nanostructures on the surface of glassy carbon under laser exposure. *Quantum Electronics* 2007; 37(11):1051-1055.
- [3]. Abramov D.V., Arakelian S.M., Galkin A.F., Klimovsky II, Kucherik A.O., Prokoshev V.G. Nanostructures on the surface of graphite samples in a laser radiation field. *Nano- and microsystem technology*2007; 4: 39-40.
- [4]. Abramov D. V., Arakelian S. M., Galkin A. F. et al. Melting of carbon heated by concentrated laser radiation in air at atmospheric pressure and a temperature not exceeding 4000 K. *JETP Letters* 2006; 84 (5): 315-319.
- [5]. Feinmann R.P., Hibbs A.R. *Quantum Mechanics and Path Integrals*. McGraw – Hill Book Company, N.Y.; 1965. 384p.
- [6]. Jirauschek Christian. Accuracy of Transfer Matrix Approaches for Solving the Effective Mass Schrodinger Equation, *IEEE, J. Quantum Electron* 2009; 45: 1059-1067
- [7]. Landau L.D., Lifshits E.M. *Theoretical physics. Volume 8: Electrodynamics of continuous media. 4th ed., M.: Fizmatlit. 2005. 652 p.*
- [8]. Demikhovsky V. Ya., Vugalter G. A. *Physics of quantum low dimensional structures. M.: Logos. 2000. 248 p.*
- [9]. Kresin V.Z., Ovchinnikov Yu.N..Shell structure and strengthening of superconducting pair correlation in nanoclusters. *Phys. Rev. B* 2006; 74:449-458.
- [10]. Zong, A., Kogar, A., Bie, Y. et al. Evidence for topological defects in a photoinduced phase transition. *Nature Phys*2019; 15:27–31.
- [11]. Arakelian S.M., Khudaberganov T.A., Istratov A.V., et al. Topological laser-induced quantum states in nanocluster structures: fundamental effects and possible applications (electrophysics and optics). *Optics and Spectroscopy* 2019; 7: 125.
- [12]. Arakelian S.M., Kucherik A.O., Khudaberganov T.A., Bukharov D.N..Modeling of macroscopic quantum states in functional properties of laser-induced 4D topological nanoclusters in thin films on a surface.*Bulletin of Russian Academy of Science. Physical Series* 2020; 84(3): 322-327.

S.M. Arakelian, et. al. "Nanocluster topological engineering of thin films by laser-hybrid technologies." *The International Journal of Engineering and Science (IJES)*, 9(7), (2020): pp. 62-70.